Impurity diffusion of ^{141}Pr in $LaMnO_3$, $LaCoO_3$ and $LaFeO_3$ materials

Marián Palcut,†[a] Jens S. Christensen,[b] Kjell Wiik[a] and Tor Grande*[a]

Received 30th May 2008, Accepted 25th July 2008
First published as an Advance Article on the web 24th September 2008
DOI: 10.1039/b808789j

The impurity diffusion of Pr^{3+} in dense polycrystalline $LaMnO_3$, $LaCoO_3$ and $LaFeO_3$ was studied at 1373–1673 K in air in order to investigate cation diffusion in these materials. Cation distribution profiles were measured by secondary-ion mass spectrometry and it was found that penetration profiles of Pr^{3+} had two distinct regions with different slopes. The first, shallow region was used to evaluate the bulk diffusion coefficients. The activation energies for bulk diffusion of Pr^{3+} in $LaMnO_3$, $LaCoO_3$ and $LaFeO_3$ were 126 ± 6, 334 ± 68 and 258 ± 75 kJ mol^{-1}, respectively, which are significantly lower than previously predicted by atomistic simulations. The bulk diffusion of Pr^{3+} in $LaMnO_3$ was enhanced compared to $LaCoO_3$ and $LaFeO_3$ due to higher concentrations of intrinsic point defects in $LaMnO_3$, especially La site vacancies. Grain-boundary diffusion coefficients of Pr^{3+} in $LaCoO_3$ and $LaFeO_3$ materials were evaluated according to the Whipple–Le Claire equation. Activation energies for grain-boundary diffusion of Pr^{3+} in $LaCoO_3$ and $LaFeO_3$ materials were 264 ± 41 kJ mol^{-1} and 290 ± 36 kJ mol^{-1} respectively. Finally, a correlation between activation energies for cation diffusion in bulk and along grain boundaries in pure and substituted $LaBO_3$ materials (B = Cr, Fe, Co) is discussed.

Introduction

Materials based on perovskite-type $LaBO_3$ oxides (B = Cr, Mn, Fe, Co) are widely used as high temperature devices since the appropriate substitution with alkaline earth metals and 3d-elements can tailor their transport properties.[1–3] Strontium-doped lanthanum chromites and manganites, for example, are state-of-the-art interconnect and cathode materials, respectively, in solid oxide fuel cells.[4–7] Sr- and Fe-substituted lanthanum cobaltites are valuable as oxygen-permeable membranes and other electrochemical devices.[8,9] These devices operate under various thermodynamic gradients. The thermodynamic forces applied at high temperatures may induce a significant cation displacement leading to structural changes and degradation over time.[10,11] To avoid these undesirable effects and achieve an optimal performance of the device, knowledge of cation diffusion is essential. It is generally observed that cations move significantly slower than oxygen in perovskite-type oxides and thus, cation diffusion limits a number of mass transport processes.[12,13] It is, therefore, surprising to realize that only a few studies have been previously devoted to experimental determination of cation diffusion coefficients. Pure and substituted $LnCrO_3$ (Ln = La, Y, Nd)[14–22] and $LnFeO_3$ (Ln = La, Y, Gd, Nd)[23–27] materials are the most studied materials in this respect. Cation diffusion in simple oxides has been studied by diffusion couple measurements, tracer diffusion and inter-diffusion experiments (see ref. 28 for review).

La^{3+} diffusion in $LaMnO_3$ and $LaCoO_3$ materials has previously not been studied experimentally. $LaMnO_3$ is known to possess large deviations from the nominal stoichiometry.[29,30] This leads to formation of cation vacancies on both La and Mn sites, tending more towards La vacancies at high temperatures. Interstitial defects are unfavourable due to the close atomic packing in the perovskite lattice. The examination of cation transport in $LaMnO_3$ by atomistic simulation techniques suggests that the lanthanum diffusion is likely to take place by a vacancy migration between neighbouring sites.[31,32] Calculated migration energy of La vacancy is 3.93 eV (379 kJ mol^{-1}) and increases with distortion from the cubic form.[31] Our previous experimental studies, focused on the diffusion-controlled kinetics of the perovskite phase formation, suggested that the mobility of both Mn^{3+} and Co^{3+} were higher than the La^{3+} mobility.[33,34] The solid-state reaction method allowed only for the determination of the diffusion coefficient for the faster moving cation. In these studies, the La^{3+} diffusion coefficients in $LaMnO_3$ and $LaCoO_3$ were not obtained.

Tracer diffusion experiments may give valuable information about cation mobility provided that the appropriate tracer is available.[35] These experiments are based on depth penetration profiles and thus, they can also be useful in determining the actual transport paths in the material.[36,37] It is known that the diffusion in ionic materials is significantly enhanced along grain boundaries and possibly also dislocations.[38–40] The relative contribution of the bulk diffusion and the grain-boundary diffusion is highly valuable since most technological applications involve polycrystalline materials. Experiments highlighting diffusion mainly in the La sublattice can be

[a] *Department of Materials Science and Engineering, Norwegian University of Science and Technology, 7491 Trondheim, Norway. E-mail: tor.grande@material.ntnu.no*
[b] *Department of Physics, University of Oslo, 0316 Oslo, Norway*
† Present address: Institute of Materials Science, Faculty of Materials Science and Technology, Slovak University of Technology, 91724 Trnava, Slovakia.

efficiently performed by the use of other lanthanoids as impurity tracers. Lanthanoid cations, Ln^{3+}, in low concentrations, especially those with similar ionic radii and ionic charge, are expected to replace lanthanum in crystal lattice without significantly changes in the crystal structure of the material.

In the present work we aim to study the impurity diffusion of Pr^{3+} in $LaBO_3$ oxides (B = Mn, Fe, Co) by secondary-ion mass spectrometry (SIMS) at 1373–1673 K in air. Praseodymium was chosen due to its similar atomic radius to lanthanum and comparable chemical properties.[41,42] Praseodymium is, next to cerium, the closest neighbour to lanthanum in the periodic table and it has only one stable, naturally occurring isotope (^{141}Pr).

Experimental

Powders of $LaMnO_3$, $LaFeO_3$ and $LaCoO_3$ were prepared by spray pyrolysis. The precursor consisted of aqueous nitrate solutions of cations mixed in stoichiometric amounts. The solution was supplied to the furnace with a speed of 2 l h^{-1}, atomized and pyrolyzed in a continuous air flow at approximately 1133 K. Collected raw powders were calcined at 1173 K for 2 h and subsequently ball-milled for 18 h in order to break agglomerates. Phase purity of $LaMnO_3$, $LaFeO_3$ and $LaCoO_3$ materials was confirmed by X-ray diffraction (SIEMENS D5005, Siemens Germany). No extra diffraction lines due to secondary phases could be observed in any of the three materials. The diffraction lines could be indexed to the space group reported for the three compounds, $R\bar{3}c$ ($LaMnO_3$, $LaCoO_3$) and *Pnma* ($LaFeO_3$) and refined lattice parameters for the three compounds $LaFeO_3$, $LaCoO_3$ and $LaMnO_3$ were in good accord with data reported in the PDF database. The X-ray diffraction (XRD) data for the compounds are given in Fig. 1.

Fine powders were shaped into cylindrical green bodies (10 mm in diameter, 2–3 mm thick) by uniaxial ($LaFeO_3$ and $LaCoO_3$) or isostatic pressing ($LaMnO_3$). Ethyl cellulose (0.7 weight%) was needed to improve the strength of the green body. The pellets of $LaFeO_3$ and $LaMnO_3$ materials were sintered at 1723 K for 2 h in air, while the $LaCoO_3$ pellets were sintered in air at 1523 K for 6 h. The final densities of the pellets, measured by the Archimedes method, were 6.32 ± 0.05, 6.54 ± 0.03 and 6.71 ± 0.05 g cm^{-3} for $LaMnO_3$, $LaFeO_3$ and $LaCoO_3$ respectively. These values correspond to 96.2, 98.5 and 92.0% of crystallographic densities for $LaMnO_3$, $LaFeO_3$ and $LaCoO_3$ respectively. The porosity of the pellets was observed to be essentially only closed porosity. Microstructure of the materials was studied by low vacuum scanning electron microscope (Hitachi S3500N). Grain size was estimated from the number of grain boundaries observed per distance unit of thermally etched surfaces. Dense pellets were ground and polished down to 0.25 μm with a diamond paste to achieve a homogeneous and smooth surface necessary for diffusion experiments.

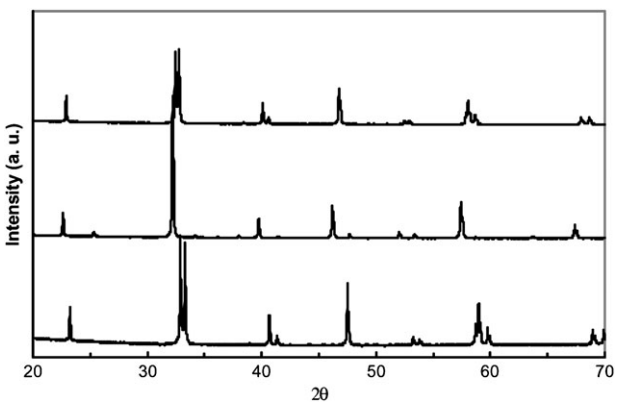

Fig. 1 X-Ray diffraction patterns for the $LaMnO_3$ (upper), $LaFeO_3$ (middle) and $LaCoO_3$ (lower) materials. The space groups are the following: $R\bar{3}c$ ($LaMnO_3$, $LaCoO_3$) and *Pnma* ($LaFeO_3$) and refined lattice parameters for the three compounds are (in Å): $LaFeO_3$ (a = 5.565, b = 5.554, c = 7.864), $LaCoO_3$ (a = 5.444, c = 13.095) and $LaMnO_3$ (a = 5.517, c = 13.332).

Diffusion source was prepared from an aqueous $Pr(NO_3)_3$ solution (c = 0.05 mol dm^{-3}). Three droplets of the solution were placed on a sample's surface and solvent was slowly evaporated at 393 K. This treatment provided a uniform, approximately 1 μm thick layer of Pr^{3+}. Samples were slowly heated to 743 K to remove volatile nitric oxides and transform praseodymium nitrate into the oxide. Samples were finally annealed at 1373, 1473, 1573 and 1673 K in air for 20, 5, 2 and 1 h respectively. Heating and cooling rates were both 600 K h^{-1}. At the conditions of the annealing the tracer source was a single oxide phase with the valence of Pr close to Pr(III).

Cation distribution in $LaMnO_3$, $LaFeO_3$ and $LaCoO_3$ materials was studied by secondary-ion mass spectrometry (SIMS) using a CAMECA ims 7f instrument. The area of 200 × 200 μm was sputtered with a ~500 nA O_2^+ primary beam (10 keV) in order to create a rectangular crater. The signal from the crater was optically gated—only the signal from the inner area of the crater with dimensions of approximately 60 × 60 μm was monitored in order to avoid negative interferences (edge and wall effects). The intensity of the signal was measured by switching between the secondary ion signals of different elements since the magnetic sector of the instrument could register only one element at a time. In the case of $LaFeO_3$ a neutralizing electron beam was used to compensate for the materials poor electrical conductivity. The intensity of the signal for each element was obtained as a function of the sputtering time. The final intensity profiles of the impurity tracer were normalized by the concentration of one of the matrix elements to compensate for variations instrumental variations. The depth of the crater was measured with a surface profilometer (Dektak 8). A depth penetration profile was calculated assuming a constant erosion rate of the material.

Results

The microstructures of the $LaMnO_3$, $LaFeO_3$ and $LaCoO_3$ materials prepared for the diffusion experiments are shown in Fig. 2 and 3. Both $LaMnO_3$ and $LaFeO_3$ (Fig. 2) were fully dense after sintering at temperatures above 1673 K. The average grain size was 2.5 ± 0.3 μm for $LaMnO_3$ and 2.9 ± 0.4 μm for $LaFeO_3$. Complete densification of $LaCoO_3$ was more complicated due to the rapid grain growth and corresponding trapping of spherical pores inside the grains at

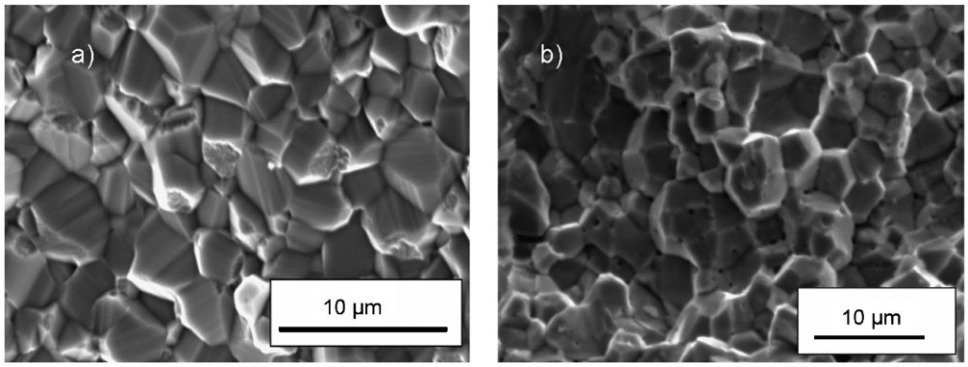

Fig. 2 Fracture surfaces showing the microstructure of (a) $LaMnO_3$ and (b) $LaFeO_3$ after sintering at 1723 K for 2 h.

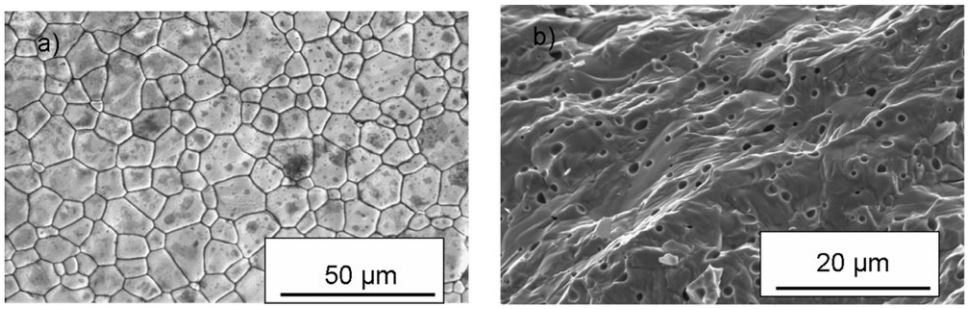

Fig. 3 (a) Grain size and (b) fracture surface of $LaCoO_3$ after sintering at 1523 K for 6 h.

high temperatures. Nevertheless, it was possible to obtain a dense material, with only closed porosity, after sintering at 1523 K for 6 h (Fig. 3). The average grain size of $LaCoO_3$ was 7.9 ± 1.0 μm. The porosity of all materials was closed (Fig. 2 and 3), and any penetration of the diffusion source into open pores could be excluded. As shown later the diffusion profiles of Pr did not provide any signature of penetration of the Pr source into open pores.

A typical crater resulting from ion sputtering is given in Fig. 4. The surface roughness of the bottom of the crater didn't exceed ±2 μm.

Typical element distribution profiles obtained by SIMS are given in Fig. 5. Signals of matrix elements (La and Mn, Fe and Co) were measured in all samples. Since the concentration of the matrix elements (Mn, Fe and Co) in the materials was assumed to be constant, any variation in their signals reflected mostly the instrumental variations during the measurements. The signals of elements in $LaFeO_3$ were significantly lower compared to the $LaMnO_3$ and $LaCoO_3$ materials due to the low electrical conductivity of $LaFeO_3$.

In most of the impurity depth profiles two distinct regions with different slopes could be recognized. The first part of the diffusion profile (region 1) was attributed to the parallel bulk and grain-boundary diffusion. The first region for the $LaMnO_3$ samples was significantly deeper and less steep compared to the $LaFeO_3$ and $LaCoO_3$ materials (Fig. 5a). This behaviour reflects enhanced praseodymium diffusion in $LaMnO_3$ relative to the two other materials. Both $LaCoO_3$ and $LaFeO_3$ showed similar behaviour with a relatively shallow first part of the diffusion profile followed by a broad second region (region 2)

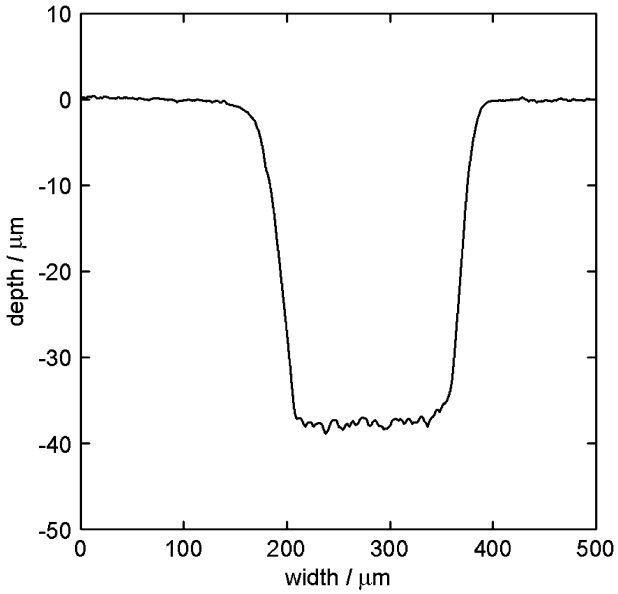

Fig. 4 Depth profile of a crater after ion sputtering illustrated on the $LaCoO_3$ specimen. Total time of sputtering was 6 h.

with a significantly smaller slope (Fig. 5). Praseodymium diffusion was studied at four different temperatures. The results obtained at 1373, 1473 and 1673 K had the same characteristic features as those already given in Fig. 5.

Diffusion in polycrystalline materials takes place simultaneously inside the grains (in the crystal lattice) and along grain

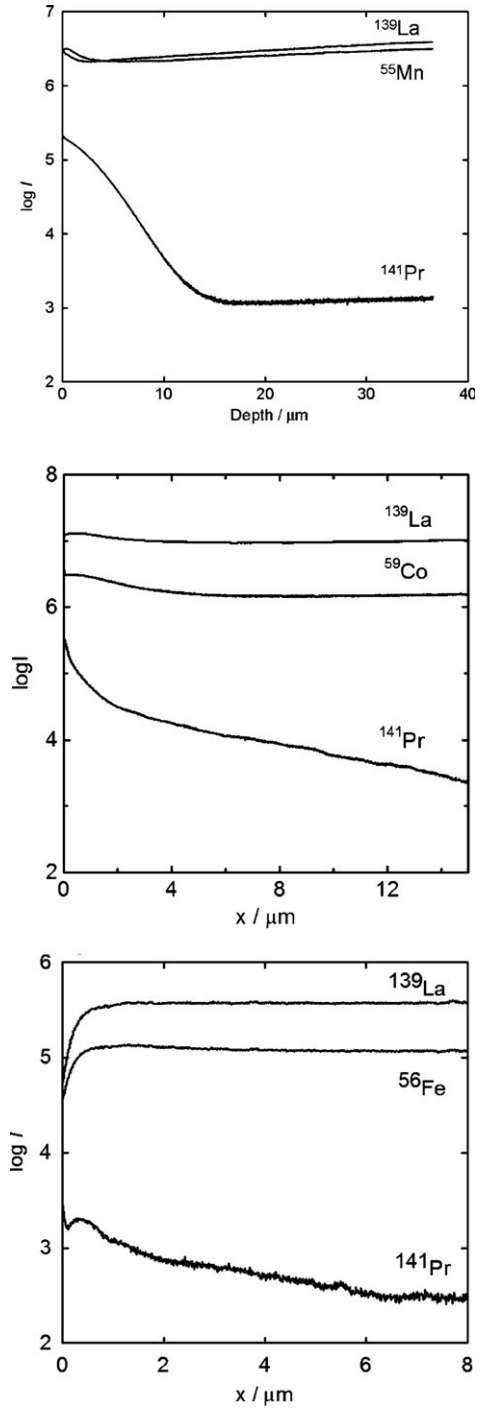

Fig. 5 Element depth profiles in $LaMnO_3$ (top), $LaCoO_3$ (middle) and $LaFeO_3$ (bottom) after the thermal anneal of praseodymium at 1573 K for 2 h in air.

boundaries. The apparent diffusion coefficient, D_{eff}, can be given by Hart's equation,[43]

$$D_{eff} = gD_{GB} + (1 - g)D_L , \quad (1)$$

where D_{GB} and D_L are the grain-boundary and lattice (bulk) diffusion coefficients, respectively and g is the fraction of atomic sites that are situated at the grain boundaries (or dislocations). The fraction of atomic sites at the grain boundaries can be estimated by the volume fraction of grain boundaries in the polycrystal. Since $g \ll 1$, eqn (1) simplifies to $D_{eff} \approx D_L + gD_{GB}$. It is seldom possible, however, to completely decouple the grain-boundary diffusion from the bulk diffusion due to the leakage of diffusing species from boundary to the adjoining grains. Harrison[44] provided the analysis of the problem using a model of parallel grain boundaries. This model distinguishes three limiting cases of diffusion kinetics. In type A, the extensive lattice and grain-boundary diffusion occur and they are mixed across the grains. In type B kinetics, fast diffusion along the grain boundaries is accompanied by a small leakage of the diffusing species into grains. Finally, in the type C diffusion kinetics, the lattice diffusion is completely eliminated.

Region 1 was used to estimate the lattice diffusion coefficient of ^{141}Pr in the $LaBO_3$ materials (B = Mn, Fe, Co). The solution of the diffusion equation

$$\frac{\partial c(x,t)}{\partial t} = D_1 \frac{\partial^2 c(x,t)}{\partial x^2} \quad (2)$$

is for diffusion from a thin-film source given as[45]

$$c(x,t) = c_0(t) \exp\left(-\frac{x^2}{4D_1 t}\right) \quad (3)$$

where $c(x,t)$ is the concentration of the diffusing species, t is the annealing time, x is the distance from the surface, $c_0(t)$ is the surface concentration of diffusant and D_1 is the apparent diffusion coefficient in region 1. The ratio $\frac{c(x,t)}{c_0(t)}$ was replaced by the intensity ratio of ^{141}Pr signal since the intensity was assumed to be proportional to concentration. Representative fit to the experimental data are shown in Fig. 6. The fitted slopes of $\log(\frac{I}{I_0})$ *vs.* x^2 obtained for the three materials are given in Table 1.

Region 2 was used to obtain data on grain-boundary diffusion of ^{141}Pr according to the Whipple–Le Claire equation,[37,46,47]

$$s\delta D_{GB} = 0.3292\sqrt{\frac{D_L}{t}}\left(-\frac{\partial \log c}{\partial x^{6/5}}\right)^{-5/3} \quad (4)$$

where s is a segregation factor and δ is the grain-boundary width. First, slope of $\log(\frac{I}{I_0})$ *vs.* $x^{1.2}$ plot in region 2 was obtained. The triple product $s\delta D_{GB}$ was then calculated assuming that $D_L = D_1$. Finally the critical parameters, α and β, were calculated according to equations[37]

$$\alpha = \frac{s\delta}{2\sqrt{D_L t}} \quad (5)$$

$$\beta = \frac{s\delta D_{GB}}{2D_L\sqrt{D_L t}} \quad (6)$$

$s\delta = 10^{-7}$ cm was adopted in order to calculate α. Representative fit to the experimental data for two of the materials are shown in Fig. 6. The numerical values for fit to the experimental data are given in Table 1. The grain-boundary diffusion coefficients in $LaMnO_3$ were not evaluated since bulk diffusion was dominating and the second region is suggested to reflect only the impurity level of Pr in the material.

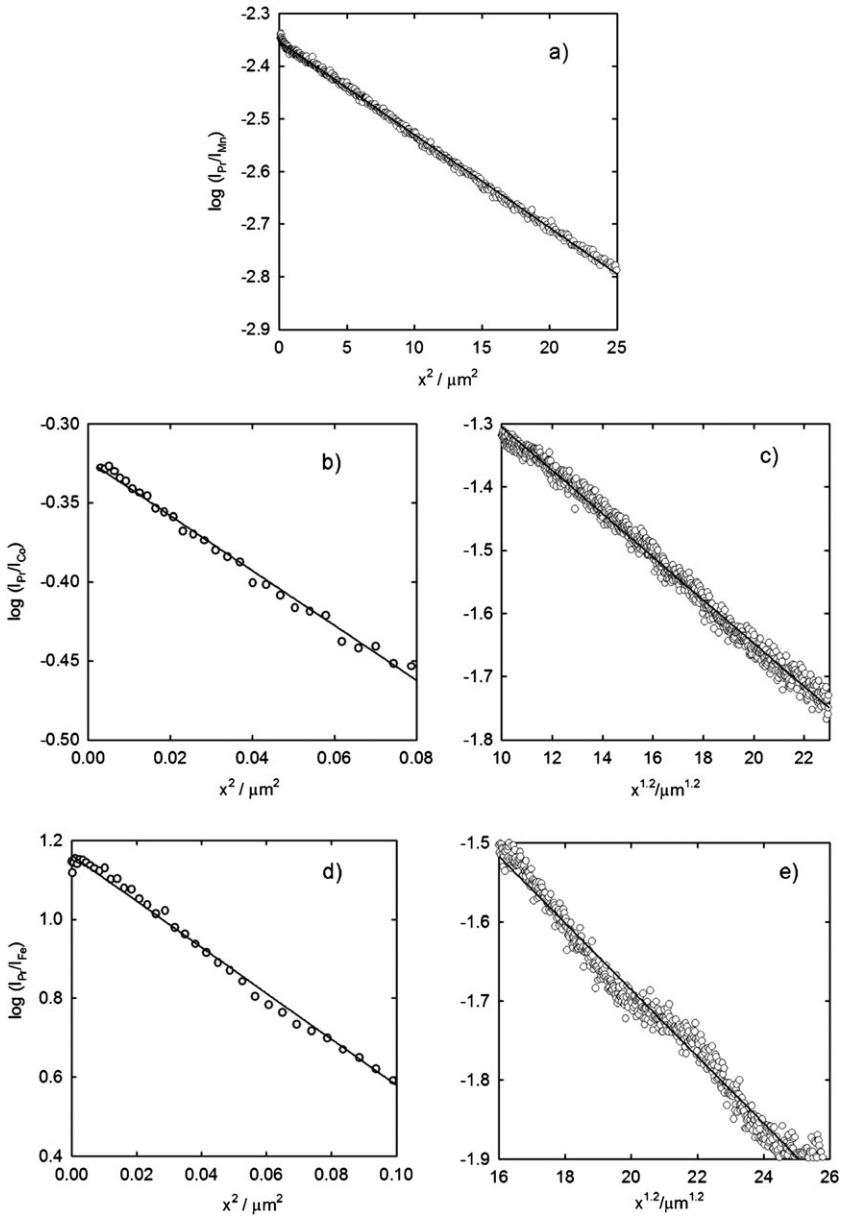

Fig. 6 Penetration profiles of the Pr^{3+} cations in (a) $LaMnO_3$, (b) and (c) $LaCoO_3$, (d) and (e) $LaFeO_3$ at 1673 K. The fitted curves are given for the respective bulk and grain-boundary regions. The intensity of Pr^{3+} was normalized by the intensity of one of the matrix elements to compensate for instrumental variations during sputtering.

Discussion

1. Bulk diffusion

Praseodymium is an impurity element in $LaBO_3$ materials. It is, therefore, of interest to compare the influence of Pr^{3+} on the structural properties of the $LaBO_3$ materials. Praseodymium replaces lanthanum in the crystal lattice. Nevertheless, it has a smaller ionic radius which reduces the Goldschmidt tolerance factor and enhances the distortion from the ideal cubic perovskite structure. Crystal structure of $La_{1-x}Pr_xCoO_3$ single crystals has been recently studied by Kobayashi *et al.*[48] The $La_{1-x}Pr_xCoO_3$ materials are rhombohedral for $0 \leq x \leq 0.3$ and orthorhombic for $0.7 \leq x \leq 1$. The lattice volume decreases monotonically with increasing Pr content due to the smaller ionic radius of Pr^{3+}. Structural properties of $La_{1-x}Pr_xMnO_{3+\delta}$ have been studied by Dyakonov *et al.*[49] $La_{1-x}Pr_xMnO_{3+\delta}$ has a rhombohedral structure for $x = 0$, orthorhombic with small Jahn–Teller distortion of MnO_6 octahedra for $0.1 < x < 0.6$ and highly distorted orthorhombic modifications for $x > 0.6$. The effect of Pr on lattice distortion is minimal at concentrations below 10%. Since the praseodymium concentration in the samples was significantly lower than La content (Fig. 5), the effect of praseodymium on crystal structure of $LaBO_3$ materials can be neglected.

The diffusion coefficients for Pr^{3+} in $LaBO_3$, D, may be expressed by an Arrhenius law

$$D = D_0 \exp\left(-\frac{E_A}{RT}\right) \quad (7)$$

Table 1 Lattice and grain-boundary diffusion data for ^{141}Pr in $LaMnO_3$, $LaFeO_3$ and $LaCoO_3$

T/K	t/h	$-\frac{\partial \log(I_{Pr}/I_M)}{\partial x^2}\Big/\mathrm{cm}^{-2}$	$D_L/\mathrm{cm}^2\ \mathrm{s}^{-1}$	$-\frac{\partial \log(I_{Pr}/I_M)}{\partial x^{1.2}}\Big/\mathrm{cm}^{-1.2}$	$s\delta D_{GB}/\mathrm{cm}^3\ \mathrm{s}^{-1}$	α	β
$LaMnO_3$							
1373	20	$(5.92 \pm 0.07) \times 10^5$	6.39×10^{-13}	—		—	—
1473	5	$(9.93 \pm 0.05) \times 10^5$	1.52×10^{-12}	—	—	—	—
1573	2	$(1.37 \pm 0.01) \times 10^6$	2.79×10^{-12}	—	—	—	—
1673	1	$(1.63 \pm 0.01) \times 10^6$	4.63×10^{-12}	—	—	—	—
$LaCoO_3$							
1373	20	$(21.6 \pm 1.4) \times 10^8$	1.74×10^{-16}	2302 ± 8	4.04×10^{-17}	0.0141	32.7×10^3
1473	5	$(2.76 \pm 0.04) \times 10^8$	5.46×10^{-15}	2316 ± 6	4.47×10^{-17}	0.00505	4.13×10^3
1573	2	$(4.08 \pm 0.25) \times 10^8$	9.24×10^{-15}	2596 ± 4	7.60×10^{-16}	0.00613	5.05×10^3
1673	1	$(1.63 \pm 0.03) \times 10^8$	4.63×10^{-14}	2157 ± 7	3.59×10^{-15}	0.00387	2.74×10^3
$LaFeO_3$							
1373	20	$(21.3 \pm 1.2) \times 10^8$	1.77×10^{-16}	2448 ± 15	3.67×10^{-17}	0.0141	29.1×10^3
1473	5	$(37.6 \pm 3.1) \times 10^8$	4.01×10^{-16}	2237 ± 7	1.28×10^{-16}	0.0186	59.7×10^3
1573	2	$(44.1 \pm 5.6) \times 10^8$	8.55×10^{-16}	1616 ± 7	5.10×10^{-16}	0.0201	12.0×10^3
1673	1	$(5.54 \pm 0.08) \times 10^8$	1.36×10^{-14}	1349 ± 4	3.89×10^{-15}	0.00714	20.4×10^3

where D_0 is a pre-exponential factor, E_A an activation energy and the other symbols have their usual meaning. From the atomistic point of view, established for diffusion in metals, the activation energy reflects a sum of the enthalpies for vacancy formation and migration and the pre-exponential factor is a product of factors reflecting probability of the individual vacancy jumps.[35,50] The bulk diffusion coefficients of Pr^{3+} in the $LaMnO_3$, $LaFeO_3$ and $LaCoO_3$ materials are compared in Fig. 7. The diffusion coefficients decrease in the following order: $LaMnO_3 \gg LaCoO_3 > LaFeO_3$. The Arrhenius activation energies are 126 ± 6, 334 ± 68 and 258 ± 75 kJ mol^{-1} for $LaMnO_3$, $LaCoO_3$ and $LaFeO_3$ respectively. Pr^{3+} diffusion in $LaMnO_3$ is significantly enhanced. Since $LaMnO_3$ has large deviations from stoichiometry,[30] this observation is not unexpected. In the following discussion we shall compare the experimental cation diffusivities in $LaMnO_3$ with predictions from atomistic simulations.

Experimental diffusion coefficients of Pr^{3+} and Mn^{3+} cations in $LaMnO_3$ are compared in Fig. 8. Activation energy for Mn^{3+} transport, determined by diffusion couple experiments, is 280 ± 40 kJ mol^{-1}.[33] The activation energy for Pr^{3+} transport is significantly lower than the activation energy for

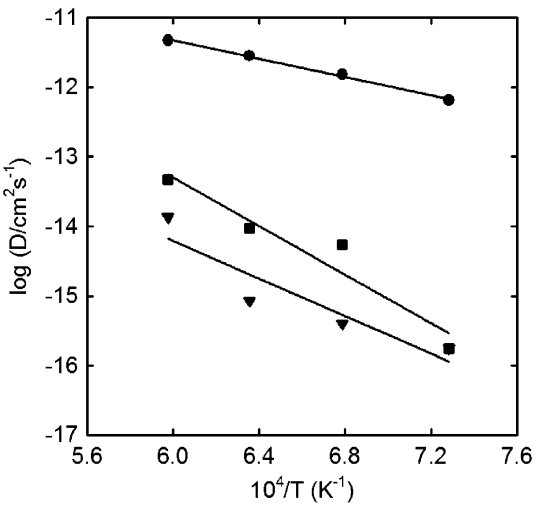

Fig. 7 Bulk diffusion coefficients of praseodymium cations in $LaMnO_3$ (●), $LaCoO_3$ (■) and $LaFeO_3$ materials (▼) in air.

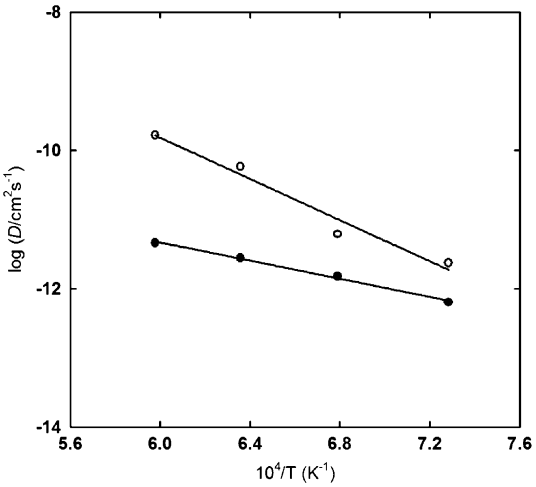

Fig. 8 Cation diffusion coefficients in $LaMnO_3$ in air: Pr bulk (●), Mn (○).[33]

Mn^{3+} diffusion. Ln^{3+} diffusion in perovskites is most likely to take place by a vacancy migration mechanism between neighbouring sites. Mn migration mechanism, however, is probably more complicated since an oxygen ion is situated between two neighbouring Mn sites. Reported activation energies for La vacancy migration in $LaMnO_3$ based on atomistic simulations are 3.93 eV (379 kJ mol^{-1}) for a cubic and 4.14 eV (400 kJ mol^{-1}) for a rhombohedrally distorted perovskite lattice.[31] Corresponding activation energies for Mn vacancy diffusion were 14.71 eV (1420 kJ mol^{-1}) for cubic and 15.73 eV (1520 kJ mol^{-1}) for rhombohedral $LaMnO_3$.[31] We suggest that Mn^{3+} and Ln^{3+} diffusion in $LaMnO_3$ occur by vacancy mechanism between neighbouring sites, but cation migration in $LaMnO_3$ is probably facilitated due to the significant amount of intrinsic point defects on cation sites in the crystal lattice.

The non-stoichiometry of $LaMnO_3$ is well known (more precisely written $La_{1-\delta}Mn_{1-\delta}O_3$ for La : Mn ratio equal to 1). Experimental results show that the oxidative non-stoichiometry leads to the formation of cation vacancies on both La and Mn sites.[51–53] $LaMnO_3$ has a solid solubility range that is temperature- and p_{O_2}-dependent.[30,33] The sublattice occupation of $LaMnO_3$ was recently studied by neutron diffraction.[54] In the

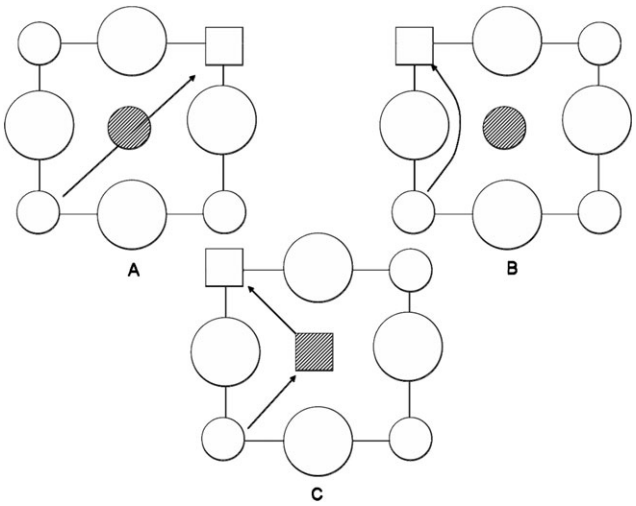

Fig. 9 Possible jumping mechanisms for Mn^{3+} cations in $LaMnO_3$ projected to the (100) plane.[31] Mn cations are represented by small open circles, Mn vacancies by small open squares, oxygen anions by large open circles, La cations by line-shaded circles and La vacancies by line-shaded squares.

course of the Rietveld refinement of these data, several models of the different site occupancy were tested. The analysis showed that the structure of La-deficient material with a nominal cation composition La : Mn = 0.91 : 1 could be given as $[La_{0.922}Mn_{0.013}]MnO_3$.[54] This result leads to the conclusion that Mn cations may occupy also vacant La sites. Mn diffusion between neighbouring sites in $LaMnO_3$ could be, therefore, facilitated by jumps *via* vacant La sites. Transport paths for the migration of Mn cations in $LaMnO_3$ have been recently proposed.[31] The projections into the (100) plane with and without La vacancies are compared in Fig. 9.[31] Mechanism A indicate a diagonal mechanism in the presence of La cations,[31] mechanism B reflects an energetically easier curved transport path around O anions[31] and mechanism C shows a facilitated Mn transport path in the presence of La vacancies. Note that the La, Mn and O ions are not situated in the same plane. La ions are in the plane behind and above the plane formed by Mn and O ions.

The impurity diffusion coefficients of Pr^{3+} are lower than the chemical diffusion coefficients of Mn^{3+} in $LaMnO_3$ of about one order of magnitude (Fig. 8). Platinum markers introduced in diffusion couple experiments showed that chemical diffusion of La^{3+} was significantly slower than Mn^{3+} diffusion.[33] It was shown that $LaMnO_3$ formed in the course of reaction between La_2O_3 and Mn_3O_4 phases had significant composition gradients.[33] At the phase boundary with La_2O_3 it had La excess, and correspondingly, low concentration of La vacancies.[33] Material prepared for tracer diffusion experiments, on the other hand, was homogeneous also evidenced by the signals of ^{55}Mn and ^{138}La which did not significantly vary over the entire sputtering process (Fig. 5). The difference between the chemical and tracer diffusion coefficients of Ln^{3+} cations in $LaMnO_3$ is therefore proposed to be related to the varying concentration of La vacancies dependent on the activity of La_2O_3 in $LaMnO_3$. It has also been observed that the cation diffusion coefficients obtained by tracer diffusion experiments had lower activation energies.[34] This is probably owing to the fact that, in tracer diffusion experiments, material with its equilibrium number of vacancies is first prepared at a high temperatures and then annealed with a tracer at lower temperatures. If the vacancy concentration is frozen-in at lower temperatures, the activation energy from tracer diffusion experiments may reflect only the enthalpy for vacancy migration. Activation energies extracted from solid state reaction kinetics are higher since they are proposed to reflect the contribution from both the vacancy formation and the migration of ions.

Bulk diffusion coefficients of Pr^{3+} in $LaFeO_3$ and $LaCoO_3$ are lower comparing to $LaMnO_3$ (Fig. 7). Activation energies are 334 ± 68 kJ mol^{-1} for $LaCoO_3$ and 258 ± 75 kJ mol^{-1} for $LaFeO_3$ respectively. The crystal structure of $LaFeO_3$ is orthorhombic, while $LaCoO_3$ is rhombohedral. The activation energies for La^{3+} vacancy migration in rhombohedral and orthorhombic perovskite from atomistic simulations are 4.14 and 4.22 eV respectively.[31] The observed difference in activation energies between $LaCoO_3$ and $LaFeO_3$ may, therefore, be due to difference in the deviation from cubic symmetry and difference in unit cell volume. Nevertheless, it has to be kept in mind that data obtained for $LaFeO_3$ are the least accurate. $LaFeO_3$ was the least conducting material and, correspondingly, a positive charge was built in the samples during the sputtering with O_2^+. Although the electron beam was used to neutralize the positive charge, charging of the specimens contributed to the low signal of the ions.

The cation diffusion coefficients in $LaFeO_3$ and $LaCoO_3$ are compared in Fig. 10 and 11. The actual cation diffusivities of Pr^{3+} in $LaCoO_3$ and $LaFeO_3$ differ by about one order of magnitude, being higher for $LaCoO_3$. The B^{3+} cation diffusion dominated over the Pr^{3+} tracer diffusion in these materials. This is in agreement with predictions from platinum marker experiments.[23,34] $LaFeO_3$ and $LaCoO_3$ are, compared to $LaMnO_3$, stoichiometric compounds ("line compounds") and do not form solid solutions. The amount of intrinsic

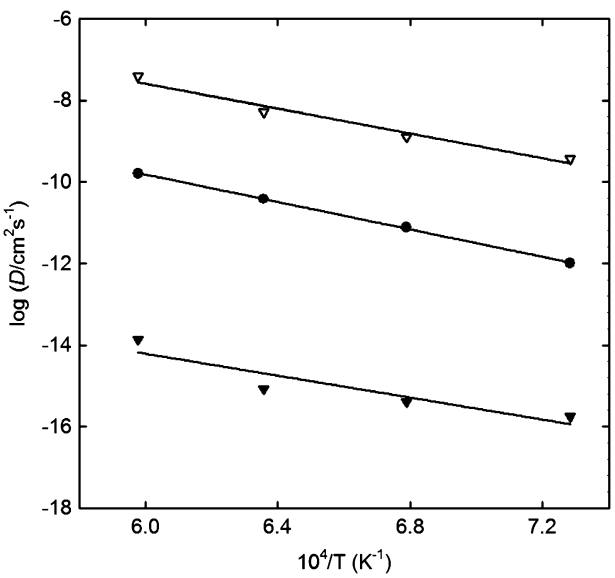

Fig. 10 Cation diffusion coefficients in $LaFeO_3$ in air: Pr bulk (▼), Pr grain boundary (▽) and Fe (●).[23]

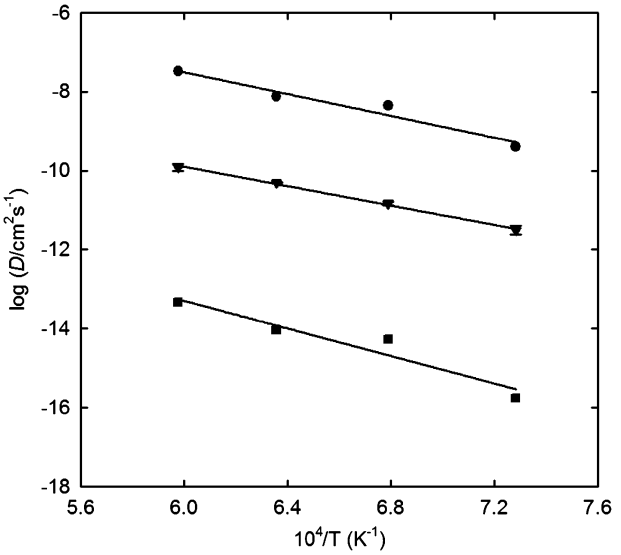

Fig. 11 Cation diffusion coefficients in $LaCoO_3$ in air: Pr bulk (■), Pr grain boundary (●) and Co (▼).[34]

cation vacancies in $LaFeO_3$ and $LaCoO_3$ are expected to be significantly lower since oxygen vacancies are dominating, while cation vacancies dominate in $LaMnO_3$.[29,30]

2. Grain-boundary diffusion

Diffusion in polycrystalline materials is a complex process requiring several elementary steps. In $LaMnO_3$, we observed that the mean diffusion length was larger than average grain size ($\sqrt{(Dt)} > d$. This observation justifies A-type diffusion kinetics.[37] Obtained diffusion coefficient (Table 1) is, therefore, an effective quantity. As a first approximation we have used the coefficient as a bulk diffusion coefficient.

Type B kinetics was observed for $LaFeO_3$ and $LaCoO_3$ materials. The mean diffusion path in region 1 was smaller than the average grain size and larger than expected grain-boundary width ($\delta \ll \sqrt{(Dt)} < d$. Grain-boundary chemistry was studied for Ca-substituted $LaCrO_3$.[55] The width of grain boundary was around 1 nm. Critical parameters for the separation of diffusion into bulk and grain boundaries were $\alpha \ll 1$ and $\beta \gg 1$ (Table 1). These values justify the use of eqn (4) for separation of diffusion into bulk and grain boundaries.[37] The β parameter reflects the relative portion of grain-boundary diffusion in materials (eqn (6)). The β values for $LaCoO_3$ are higher than the β values for $LaFeO_3$ (except the 1373 K experiment, see Table 1). The different portions of the GB diffusion in the $LaFeO_3$ and $LaCoO_3$ materials can be rationalized due to the different portions of the grain boundaries coming from different grain sizes of the materials. $LaCoO_3$ had significantly larger grain size than $LaFeO_3$ (Fig. 2 and 3) and thus, the relative portion of grain-boundary diffusion was smaller.

The grain-boundary diffusion coefficients of Pr^{3+} cations in $LaCoO_3$ and $LaFeO_3$ materials, given in Fig. 10 and 11, were calculated assuming that $s = 1$ and $\delta = 1$ nm. The grain-boundary diffusion coefficients are more than 5 orders of magnitude higher than the respective bulk diffusion coefficients (Fig. 10 and 11). The grain boundaries thus constitute a

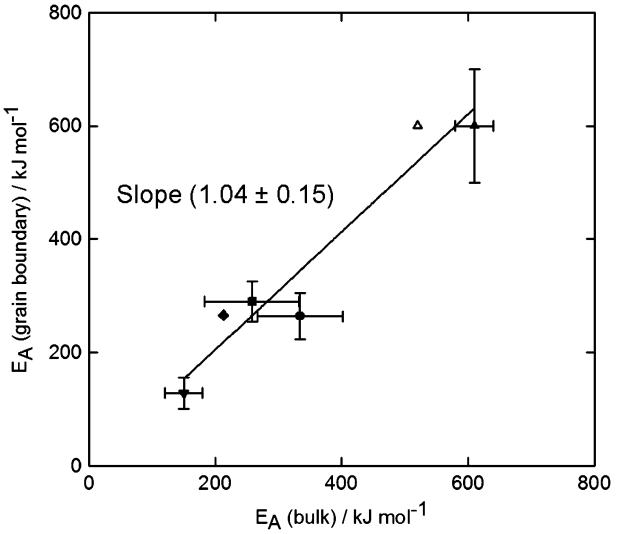

Fig. 12 Correlation between activation energies for bulk and grain-boundary cation diffusion in perovskite-type oxides: ● tracer diffusion of Pr^{3+} in $LaCoO_3$ (present data), ■ tracer diffusion of Pr^{3+} in $LaFeO_3$ (present data), ◆ tracer diffusion of Cr^{3+} in $LaCrO_3$,[22] ▼ tracer diffusion of Cr^{3+} in $La_{0.9}Sr_{0.1}FeO_{3-\delta}$,[27] ▲ diffusion of Nd^{3+} in $LaFeO_3$,[26] △ diffusion of Mn^{3+} in $La_{0.6}Sr_{0.4}Co_{0.2}Fe_{0.8}O_{3-\delta}$.[11]

rapid transport path for Pr^{3+} cations in these materials. The activation energies for grain-boundary diffusion are 264 ± 41 kJ mol^{-1} and 290 ± 36 kJ mol^{-1} for $LaCoO_3$ and $LaFeO_3$ respectively. These values are similar to the respective activation energies for bulk diffusion. The activation energies for bulk and grain-boundary diffusion for perovskite-type oxides are compared in Fig. 12. The activation energies for bulk and grain-boundary diffusion of cations in perovskite-type oxides fall into one line with a slope of 1.04 ± 0.15 irrespective of the type of experimental technique and perovskite material studied.

The relationship between activation energies for cation transport in bulk and grain boundaries has not been widely studied for oxide materials. Best to our knowledge, only one study reported relationship between activation energy for bulk and grain-boundary diffusion in cubic and tetragonal zirconia.[56] The authors found that activation energy for grain-boundary diffusion is about 0.8 of bulk diffusion.[56] This value seems to be consistent with the one found in this study and suggests that the mechanism for cation diffusion in grain boundaries could be a simple vacancy hopping between neighbouring sites. Nevertheless, further systematic studies with oxide materials are apparently needed to confirm this hypothesis. Studies dealing with the grain boundaries of these perovskite materials have recently been reported.[57] These studies could be useful in this respect since they can shed further light into the defect chemistry of grain boundaries.

Conclusion

Impurity diffusion coefficients of Pr^{3+} cations in polycrystalline $LaMnO_3$, $LaFeO_3$ and $LaCoO_3$ materials have been determined by secondary-ion mass spectrometry. Bulk and grain-boundary diffusion coefficients were obtained by fitting

the tracer penetration profiles. The activation energy for bulk diffusion is considerably lower than predicted from atomistic consideration. Bulk diffusion is significantly enhanced in $LaMnO_3$ relative to $LaFeO_3$ and $LaCoO_3$ reflecting the higher cation-vacancy concentrations in $LaMnO_3$. The similar activation energy of bulk and grain-boundary diffusion in $LaFeO_3$ and $LaCoO_3$ were found. This observation suggests that the transport mechanisms in the grains and along grain boundaries are related.

Acknowledgements

M. P. thanks Øystein S. Andersen and Trine Øyås (both from Department of Materials Science and Engineering, Norwegian University of Science and Technology, NTNU, Trondheim) for the powder preparation by spray pyrolysis. This work was co-financed by Research Council of Norway (Grant no. 158517/431, Functional oxides for energy technology), NTNU and UNIFOR Oslo.

References

1 M. A. Peña and J. L. G. Fierro, *Chem. Rev.*, 2001, **101**, 1981.
2 H. U. Anderson, *Solid State Ionics*, 1992, **52**, 33.
3 J. P. Attfield, *Chem. Mater.*, 1998, **10**, 3239.
4 N. Q. Minh, *J. Am. Ceram. Soc.*, 1993, **76**, 563.
5 J. P. P. Huijsmans, *Curr. Opin. Solid State Mater. Sci.*, 2001, **5**, 317.
6 N. P. Brandon, S. Skinner and B. C. H. Steele, *Annu. Rev. Mater. Res.*, 2003, **33**, 183.
7 L. J. Gauckler, D. Beckel, B. E. Buergler, E. Jud, U. P. Muecke, M. Prestat, J. L. M. Rupp and J. Richter, *Chimia*, 2004, **58**, 837.
8 Y. Teraoka, T. Nobunaga, K. Okamoto, N. Miura and N. Yamazoe, *Solid State Ionics*, 1991, **48**, 207.
9 V. V. Kharton, E. N. Naumovich and A. V. Nikolaev, *J. Membr. Sci.*, 1996, **111**, 149.
10 S. P. S. Badwal, *Solid State Ionics*, 2001, **143**, 39.
11 N. Sakai, T. Horita, K. Yamaji, M. E. Brito, H. Yokokawa, A. Kawakami, S. Matsuoka, N. Watanabe and A. Ueno, *J. Electrochem. Soc.*, 2006, **153**, A621.
12 J. L. Routbort, K. C. Goretta, R. E. Cook and J. Wolfenstine, *Solid State Ionics*, 2000, **129**, 53.
13 A. Domínguez-Rodríguez, M. Jiménez-Melendo, N. Chen, K. C. Goretta, S. J. Rothman and J. L. Routbort, *J. Phys. III*, 1994, **4**, 253.
14 T. Akashi, M. Nanko, T. Maruyama, Y. Shiraishi and J. Tunabe, *J. Electrochem. Soc.*, 1998, **145**, 2090.
15 K. Kawamura, A. Saiki, T. Maruyama and K. Nagata, *J. Electrochem. Soc.*, 1995, **142**, 3073.
16 T. Akashi, Y. Mizuno, M. Nanko, T. Maruyama, A. Saiki, K. Tsukui and J. Tunabe, *Mater. Trans.*, 2001, **42**, 1411.
17 T. Maruyama and T. Akashi, *Proc. Electrochem. Soc.*, 1998, **97–24**, 789.
18 J.-O. Hong, S. Miyoshi, A. Kaimai, Y. Nigara, T. Kawada and J. Mizusaki, *Proc. Electrochem. Soc.*, 2001, **28**, 49.
19 T. Horita, M. Ishikawa, K. Yamaji, N. Sakai, H. Yokokawa and M. Dokiya, *Solid State Ionics*, 1998, **108**, 383.
20 T. Horita, M. Ishikawa, K. Yamaji, N. Sakai, H. Yokokawa and M. Dokiya, *Solid State Ionics*, 1999, **124**, 301.
21 T. Horita, N. Sakai, T. Kawada, H. Yokokawa and M. Dokiya, *J. Am. Ceram. Soc.*, 1998, **81**, 315.
22 N. Sakai, K. Yamaji, T. Horita, H. Negishi and H. Yokokawa, *Solid State Ionics*, 2000, **135**, 469.
23 J. B. Smith and T. Norby, *Solid State Ionics*, 2006, **177**, 639.
24 V. Buscaglia, F. Caracciolo, C. Bottino, M. Leoni and P. Nanni, *Acta Mater.*, 1997, **45**, 1213.
25 V. Buscaglia, M. T. Buscaglia, L. Giordano, A. Martinelli, M. Viviani and C. Bottino, *Solid State Ionics*, 2002, **146**, 257.
26 J. B. Smith, T. Norby and A. Fossdal, *J. Am. Ceram. Soc.*, 2006, **89**, 582.
27 I. Wærnhus, N. Sakai, H. Yokokawa, T. Grande, M.-A. Einarsrud and K. Wiik, *Solid State Ionics*, 2004, **175**, 69.
28 R. Freer, *J. Mater. Sci.*, 1980, **15**, 803.
29 B. C. Tofield and W. R. Scott, *J. Solid State Chem.*, 1974, **10**, 183.
30 J. A. M. van Roosmalen, P. van Vlaanderen, E. H. P. Cordfunke, W. L. Ijdo and D. J. W. Ijdo, *J. Solid State Chem.*, 1995, **114**, 516.
31 R. A. De Souza, M. S. Islam and E. Ivers-Tiffée, *J. Mater. Chem.*, 1999, **9**, 1621.
32 M. S. Islam, *Solid State Ionics*, 2002, **154–155**, 75.
33 M. Palcut, K. Wiik and T. Grande, *J. Phys. Chem. C*, 2007, **111**, 813.
34 M. Palcut, K. Wiik and T. Grande, *J. Phys. Chem. B*, 2007, **111**, 2299.
35 H. Mehrer, in *Diffusion in Condensed Matter: Methods, Materials, Models*, ed. P. Heitjans and J. Kärger, Springer, Berlin, Germany, 2005, p. 3.
36 M. Martin, in *Diffusion in Condensed Matter: Methods, Materials, Models*, ed. P. Heitjans and J. Kärger, Springer, Berlin Germany, 2005, p. 209.
37 C. Herzig and Y. Mishin, in *Diffusion in Condensed Matter: Methods, Materials, Models*, ed. P. Heitjans and J. Kärger, Springer, Berlin Germany, 2005, p. 337.
38 J. H. Harding, *Interface Sci.*, 2003, **11**, 81.
39 W. Preis, *Phys. Chem. Chem. Phys.*, 2006, **8**, 2629.
40 I. V. Belova and G. E. Murch, *J. Phys. Chem. Solids*, 2003, **64**, 873.
41 G. H. Aylward and T. J. V. Findlay, *SI Chemical Data*, John Wiley & Sons, Sydney, Australia, 1971.
42 R. D. Shannon, *Acta Crystallogr., Sect. A: Cryst. Phys., Diffr., Theor. Gen. Cryst.*, 1976, **32**, 751.
43 E. W. Hart, *Acta Metall.*, 1957, **5**, 597.
44 L. G. Harrison, *Trans. Faraday Soc.*, 1961, **57**, 1191.
45 J. Crank, *Mathematics of Diffusion*, Oxford University Press, Great Britain, 1956.
46 A. D. Le Claire, *Br J Appl Phys*, 1963, **14**, 351.
47 I. Kaur, Y. Mishin and W. Gust, *Fundamentals of Grain and Interphase Boundary Diffusion*, John Wiley & Sons Ltd., Chichester, Great Britain, 1995.
48 Y. Kobayashi, T. Mogi and K. Asai, *J. Phys. Soc. Jpn.*, 2006, **75**, 104703.
49 V. Dyakonov, F. Bukhanko, V. Kamenev, E. Zubov, S. Baran, T. Jaworska-Gołąb, A. Szytuła, E. Wawrzyska, B. Penc, R. Duraj, N. Stüsser, M. Arciszewska, W. Dobrowolski, K. Dyakonov, J. Pientosa, O. Manus, A. Nabialek, P. Aleshkevych, R. Puzniak, A. Wisniewski, R. Zuberek and H. Szymczak, *Phys. Rev. B*, 2006, **74**, 24418.
50 E. P. Butler, H. Jain and D. M. Smyth, *J. Am. Ceram. Soc.*, 1991, **74**, 772.
51 L. Malavasi, C. Ritter, M. C. Mozzati, C. Tealdi, M. S. Islam, C. B. Azzoni and G. Flor, *J. Solid State Chem.*, 2005, **178**, 2042.
52 S. Miyoshi, J.-O. Hong, K. Yashiro, A. Kaimai, Y. Nigara, K. Kawamura, T. Kawada and Mizusaki, *Solid State Ionics*, 2002, **154–155**, 257.
53 S. Miyoshi, J.-O. Hong, K. Yashiro, A. Kaimai, Y. Nigara, K. Kawamura, T. Kawada and S. Mizusaki, *Solid State Ionics*, 2003, **161**, 209.
54 M. Wołcyrz, R. Horyń, F. Bourée and E. Bukowska, *J. Alloys Compd.*, 2003, **353**, 170.
55 N. Sakai, T. Tsunoda, N. Fukumoto, I. Kojima, K. Yamaji, T. Horita, M. Ishikawa, H. Yokokawa and M. Dokiya, *J. Electroceram.*, 1999, **4:S1**, 121.
56 S. Swaroop, M. Kilo, C. Argirusis, G. Borchardt and A. H. Chokshi, *Acta Mater.*, 2005, **53**, 4975.
57 P. E. Vullum, A. T. J. van Helvoort, R. Holmestad, J. Mastin, O. E. Andersen, M. A. Einarsud and T. Grande, *J. Mater. Sci.*, 2007, **42**, 6267.

